

Low temperature dielectric relaxation in ordinary perovskite ferroelectrics: enlightenment from high-energy X-ray diffraction

D A Ochoa,¹ R Levit,¹ C M Fancher,² G Esteves,² J L Jones² and J E García¹

¹ Department of Physics, Universitat Politècnica de Catalunya - BarcelonaTech, Barcelona 08034, Spain

² Department of Materials Science and Engineering, North Carolina State University, Raleigh, North Carolina 27695, USA

E-mail: jose.eduardo.garcia@upc.edu

Abstract

Ordinary ferroelectrics exhibit a second order phase transition that is characterized by a sharp peak in the dielectric permittivity at a frequency-independent temperature. Furthermore, these materials show a low temperature dielectric relaxation that appears to be a common behavior of perovskite systems. Tetragonal lead zirconate titanate is used here as a model system in order to explore the origin of such an anomaly, since there is no consensus about the physical phenomenon involved in it. Crystallographic and domain structure studies are performed from temperature dependent synchrotron X-ray diffraction measurement. Results indicate that the dielectric relaxation cannot be associated with crystallographic or domain configuration changes. The relaxation process is then parameterized by using the Vogel-Fulcher-Tammann phenomenological equation. Results allows us to hypothesize that the observed phenomenon is due to changes in the dynamic behavior of the ferroelectric domains related to the fluctuation of the local polarization.

Keywords: ferroelectrics, piezoelectric materials, dielectric response, dielectric relaxation

The macroscopic dielectric response of ferroelectric materials is closely linked to the crystallographic structure, to the ferroelectric/ferroelastic domain structure and to the dynamic behaviors of that domain structure [1]. One of the most attractive aspects of dielectric studies is that the temperature-dependent dielectric response is also sensitive to changes in the crystal structure as well as in the domain structure and/or their dynamic behavior [2]. For instance, phase transitions appear as a maximum in the real and/or imaginary permittivity versus temperature curve. In particular, the paraelectric to ferroelectric phase transition manifests as a sharp peak at a frequency-independent temperature in ordinary ferroelectrics while a wide peak at a temperature that is frequency-dependent is observed in the so-called relaxor ferroelectrics [3].

A widely studied dielectric anomaly appears at low temperatures in ordinary perovskite ferroelectrics [4-16]. In the $\text{PbZr}_{1-x}\text{Ti}_x\text{O}_3$ (PZT) system, for instance, it appears independently of the crystallographic phase as a flat region in the real part of the permittivity (ϵ'), and as a dispersion of the maximum in the imaginary part of the permittivity (ϵ'') [5]. When the PZT system is acceptor doped, the frequency-dependent maximum of ϵ'' becomes more visible [5]. However, the anomalous behavior of the permittivity seem to vanish when the material is donor doped [4-6]. A similar anomalous temperature-dependent permittivity has been reported in NaNbO_3 [10], $(\text{K},\text{Na})\text{NbO}_3$ [11], $(1-x)\text{Pb}(\text{Mg}_{1/3}\text{Nb}_{2/3})\text{O}_3$ - $x\text{PbTiO}_3$ [12], and $(1-x)\text{Pb}(\text{Zn}_{1/3}\text{Nb}_{2/3})\text{O}_3$ - $x\text{PbTiO}_3$ [13], which are not related to any change in crystallographic symmetry. More recently, low temperature dielectric relaxations have been reported in BaTiO_3 - BiScO_3 [15] and PbTiO_3 - BiScO_3 [16] systems, which were parameterized by using the Vogel-Fulcher-Tammann formalism. Guo et al. [15] referred to this phenomenon as re-entrant type relaxor behavior, since a peculiar domain structure characterized by piezoresponse force microscopy studies showed no phase contrast. Algueró et al. [16]

associated the anomaly with a low temperature phase transition that is governed by an order parameter coupled to polarization in Bi-containing perovskites.

Although the low temperature dielectric relaxation displayed in ordinary ferroelectrics has been reported for a wide number of systems [4-16], the involved mechanisms are not well understood. The universality of this phenomenon seems to be indisputable, but numerous explanations, often meaningful only for the study system, have been given about the origin of this anomalous behavior. In this work, the crystallographic and domain structure of an ordinary ferroelectric are studied in order to gain insight into the origin of this very exciting phenomenon. The work focuses attention on the PZT system, since this is a classical perovskite ferroelectric that has a well-established phase diagram and its dielectric properties have been widely studied. The composition $\text{Pb}(\text{Zr}_{0.4}\text{Ti}_{0.6})\text{O}_3$ is selected because it is far enough from the morphotropic phase boundary (MPB) of PZT system, thereby avoiding low temperature phenomena associated to phase transitions in this region [17]. $\text{Pb}(\text{Zr}_{0.4}\text{Ti}_{0.6})\text{O}_3$ is a tetragonal perovskite material for which only a cubic-to-tetragonal (on cooling) phase transition near to 690 K has been reported [18].

It is well-known that the properties of the PZT system can be easily tuned by compositional engineering. For instance, the substitution of Zr^{4+} or Ti^{4+} by pentavalent (donor) or trivalent (acceptor) cations largely modifies their physical properties. The addition of acceptor dopants generates oxygen vacancies that give rise to the formation of so-called complex (dipolar) defects, while donor dopants generate lead vacancies and reduce oxygen vacancies [19]. In this work, $\text{Pb}(\text{Zr}_{0.4}\text{Ti}_{0.6})\text{O}_3$ was doped with 1 wt. % of Fe_2O_3 (PFZT) to create a composition containing dipolar defects, and with 1 wt. % of Nb_2O_5 (PNZT) to design a dipolar defect-free composition. PFZT and PNZT compositions were prepared by conventional solid state reaction route. Sintered PFZT and PNZT samples were cut into disks of 15–16 mm in diameter and 0.8–0.9 mm in thickness, avoiding Pb inhomogeneous areas. The microstructure shows

dense polycrystals with an average grain size of $\sim 1.0 \mu\text{m}$ for PFZT and $\sim 3.0 \mu\text{m}$ for PNZT (see supplementary data). Gold electrodes are sputtered on both faces of the samples in order to perform the dielectric measurement. A precision LCR meter (Agilent E4980A) is used for measurements of the real and imaginary parts of the permittivity at several frequencies between 100 Hz and 1 MHz. Low temperature (30 K to 390 K) permittivity data were measured using a closed loop cryogenic system consisting of a helium compressor (Cryogenics 8200), a cold finger (Cryogenic model 22), a temperature controller (LakeShore model 331) and a vacuum pump (Alcatel Drytel Micro CFV100D). A temperature-controlled (Eurotherm 3216) tubular furnace (Carbolite MTF 12/38/250) was used to measure high temperature (room temperature to 800 K) permittivity data.

Figure 1 shows the measured temperature dependence of real, ϵ' , and imaginary, ϵ'' , permittivity for PNZT and PFZT at different frequencies. The high temperature dielectric anomaly in ϵ' associated to the ferroelectric-paraelectric phase transition for PNZT and PFZT is shown in figures 1(a) and 1(c). This transition is also observed in ϵ'' for PNZT (figure 1(b)), but not for PFZT (figure 1(d)), because in these materials it is concealed by high dielectric losses associated to oxygen vacancy conduction. Focusing attention on the insets, it is possible to observe the low temperature dielectric anomaly for both PFZT and PNZT. The inset in figure 1(c) highlights the anomalous behavior in ϵ' for PFZT that appears as a flat region in the ϵ' values around 240 K. The dielectric anomaly in ϵ'' for this material, understood as the maximum of ϵ'' , emerges at lower temperatures and exhibits frequency dispersion, as can be seen in the inset of figure 1(d). This behavior has been associated to the domain wall pinning effect by the presence of dipolar defects ($Fe'_{B-site} - V_O$) created by Fe^{3+} addition in the PZT matrix [4]. However, this explanation is only valid for materials containing dipolar defects, so no anomalous behavior could be expected in PNZT since no dipolar defects are present. The emergence of a dielectric anomaly in PNZT (figure 1(b)) casts doubt on the direct relation

between the dielectric anomaly and dipolar defects. It is important to point out that no low temperature anomalous dielectric behavior has been reported so far in donor-doped PZT.

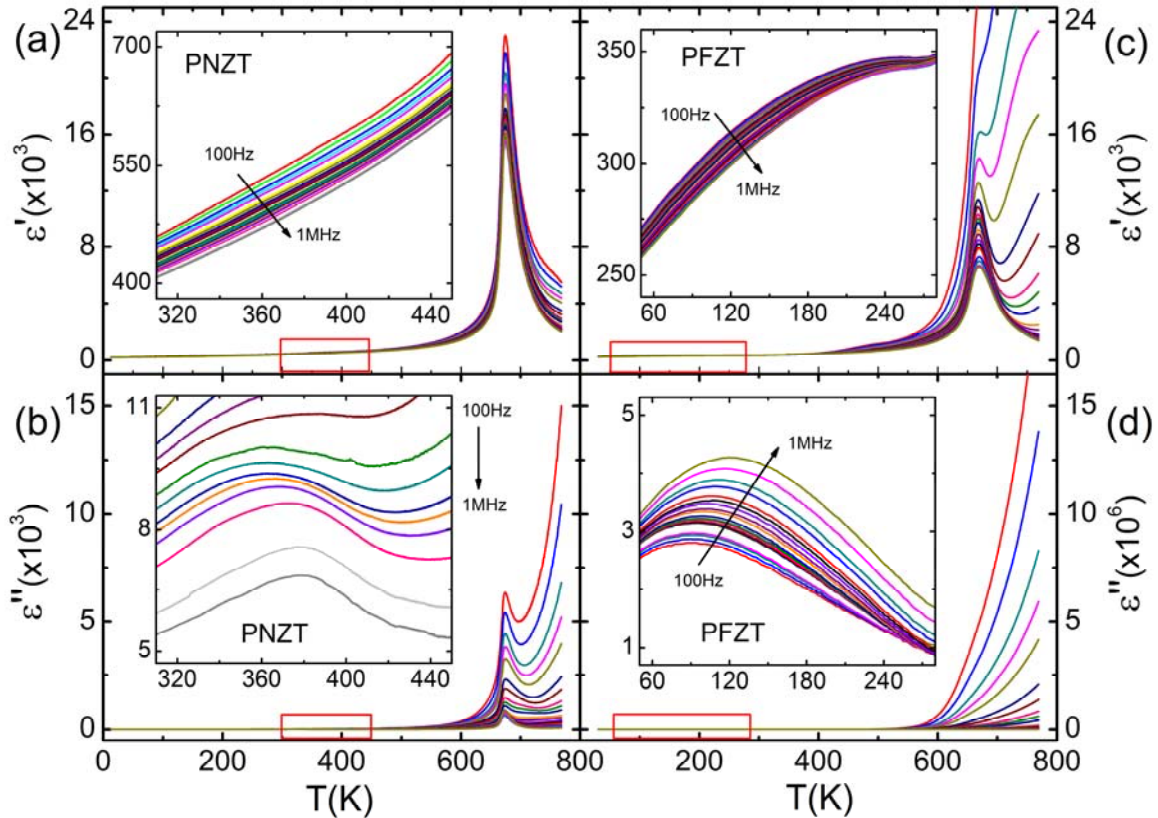


Figure 1. Real, ϵ' , and imaginary, ϵ'' , parts of the permittivity from low temperature (~ 20 K) to above the ferroelectric-paraelectric phase transition (~ 780 K) for (a-b) Nb- and (c-d) Fe-doped $\text{Pb}(\text{Zr}_{0.4}\text{Ti}_{0.6})\text{O}_3$ (PNZT and PFZT, respectively) at several frequencies. The insets display a zoom of the region highlighted with a red rectangle in each panel. Two dielectric anomalies are detected in both materials for temperature ranges, depending on the material. The dispersive character of the low temperature anomaly is clearly evidenced in the insets of ϵ'' .

Some differences between PNZT and PFZT anomalies are easily detectable. For instance, a clear $\epsilon''(T)$ peak is shown for PFZT, whereas this peak is evident only at high frequencies for PNZT. In addition, the amplitude of the peak increases with increasing frequency for PFZT but decreases for PNZT. These differences have their origin in how the thermally activated phenomena (i.e. extrinsic effects that are mainly due to domain wall motion in the PZT system) determine the dielectric response in these materials. A monotonous increment of complex permittivity (from an intrinsically low temperature dielectric constant to the vicinity of phase transition) is expected as a result of the extrinsic effect. Since the motion of domain

walls is a dynamic phenomenon (i.e. frequency-dependent), the extrinsic contribution drops as the frequency increases. Thus, dielectric constant decreases as the frequency increases for a given temperature. This effect is greater as the temperature rises (in fact, the very low temperature permittivity –intrinsic permittivity- is frequency-independent). Any other phenomenon is overlapping to that; i.e., a monotonous frequency-dependent increment of complex permittivity appears as a background in the dielectric spectra. Therefore, the observed dielectric relaxation (in both PNZT and PFZT) is actually influenced by this background. However, this has special significance for PNZT, because the dielectric relaxation emerges at a range of temperature higher than room temperature. It is for that reason that the dielectric relaxation in PNZT is then affected by a large background (large extrinsic effect), which shows a decreasing behavior with frequency. Consequently, the amplitude of the dielectric loss peak decreases in this material, although the dielectric relaxation phenomenon is purely dynamical.

High-energy, high-resolution temperature-dependent X-ray diffraction measurements were performed in order to analyze a possible crystallographic origin of the anomaly. The diffraction data were measured at beamline 11-BM of the Advanced Photon Source at Argonne National Laboratory. An X-ray wavelength of 0.4138 Å (~30 keV) was used. Diffracted X-rays were measured using an array of twelve detectors with Si (111) analyzer crystals. Samples were cooled and heated using an Oxford Cryostream (100 - 435 K) or a Cyberstar hot air blower (450 – 705 K), respectively. Some details about the structural characterization of the samples are given in the supplementary data.

Figure 2 shows the typical evolution from cubic to tetragonal structure with decreasing temperature in PNZT (figure 2(a)) and PFZT (figure 2(b)). The 200 cubic reflection splits at the Curie temperature, unveiling the structural phase transition. No structural changes below Curie temperature are detected. This suggests that both materials remain in the tetragonal

phase, revealing a non-crystallographic origin of the anomaly. The volume of the material affected by domain wall strains, which is related to domain wall density, is then estimated from the diffuse intensities between the 002 and 200 diffraction peaks [20, 21]. Figure 3 shows the percentage of the diffuse scattering (volume fraction of the material) due to domain walls for PNZT and PFZT. As may be observed, neither the values for PNZT nor the values for PFZT show any relevant changes over the whole range of temperatures, with the exception, as expected, near the ferroelectric-paraelectric phase transition temperature, where the diffuse scattering due to domain walls drops to zero. Therefore, it is possible to assume that no change in the domain configuration for temperatures below the phase transition exists, and, in particular, in the region where the dielectric relaxation emerges.

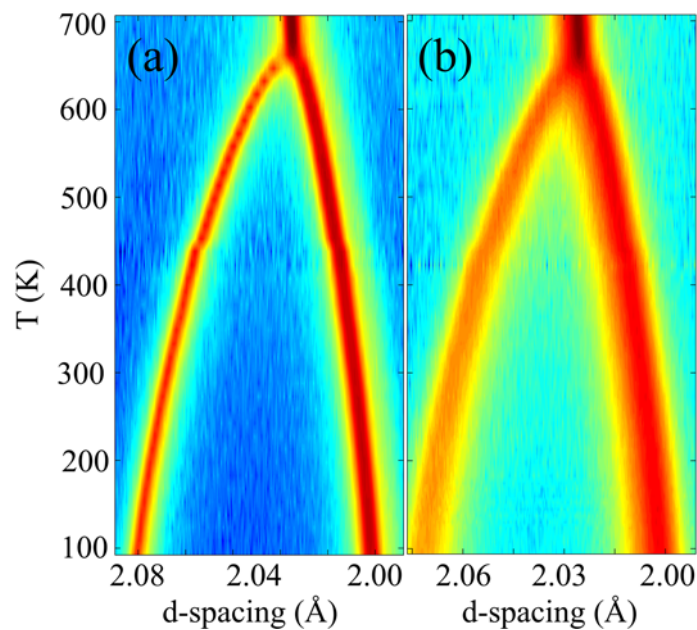


Figure 2. Contour plot obtained from the 200 Bragg reflection of the XRD patterns for (a) PNZT and (b) PFZT. When materials are heated, the tetragonal 002/200 degenerated reflection becomes the cubic 200 reflection illustrating the ferroelectric-to-paraelectric phase transition. No structural changes are observed when the materials are cooled.

The diffuse scattering difference between PNZT and PFZT may be related to the microstructure and how the microstructure defines the domain configuration in both compositions. Taking into account that the diffuse scattering due to domain walls (S_{DW}) is

proportional to domain wall density (N_d), the ratio between domain wall densities can be estimated, such that:

$$\frac{N_d^{PFZT}}{N_d^{PNZT}} = \frac{S_{DW}^{PFZT}}{S_{DW}^{PNZT}} \sim 1.7$$

Assuming that the width (w) of the ferroelectric domains in microstructured perovskite ferroelectrics can be considered proportional to the square root of the grain diameter ($w \propto \sqrt{a}$) [22], but inversely proportional to domain wall density ($w \propto \frac{1}{N_d}$) [23], the ratio between domain wall densities can also be estimated as:

$$\frac{N_d^{PFZT}}{N_d^{PNZT}} = \sqrt{\frac{a^{PNZT}}{a^{PFZT}}} \sim 1.7$$

the grain diameter being considered as the median grain size for both materials; i.e., 3.0 μm for PNZT and 1.0 μm for PFZT. The agreement between the results indicates that the difference in the diffuse scattering between PNZT and PFZT is due to a difference in the domain wall density.

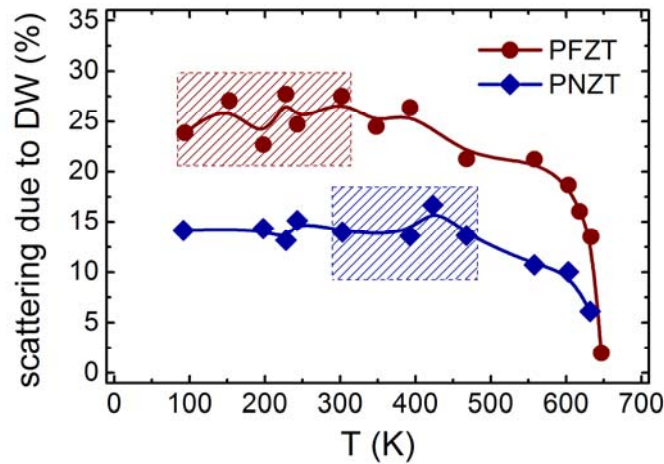


Figure 3. Percentage of diffuse scattering related to the volume of material affected by domain wall strains as a function of the temperature, for PFZT and PNZT. The drawn squares are a guide to the temperature range in which the dielectric relaxations are observed for each composition.

X-ray diffraction data analysis demonstrates that the observed dielectric anomaly in PNZT and PFZT are not associated with crystallographic or domain configuration changes. Consequently, it is reasonable to hypothesize that the observed phenomenon is due to changes in the dynamic behavior of the ferroelectric domains related to the fluctuation of an order parameter (e.g., the local polarization). Other phenomena that manifest as dielectric relaxation, such as grain boundary and contact (electrode) effects [24, 25], may emerge at a range of frequencies far from that used in this work. Also, phenomena such as interface effects and charge-carrier mobility, which are relevant for determining functional properties of heterogeneous ferroelectric systems (i.e., graded/multilayer ferroelectrics or ferroelectric superlattices), are not taking into account [26-28].

The frequency dependence of the maximum in ϵ'' is parameterized by using the Vogel-Fulcher-Tammann (VFT) phenomenological equation (see supplementary data), which is probably the most commonly used equation for fitting dielectric relaxation in ferroelectrics. Figure 4 shows the VFT fit for the relaxation data, such that the slope is related to the activation energy of the dynamic process involved. The activation energies are ~ 20 meV and ~ 3 meV for PFZT and PNZT, respectively. In order to determine the process associated to these activation energies, the dipolar energy corresponding to the different possible positions of the defect in the unit cell is estimated. This is done by assuming a simple model based on an ideal dipole placed in a ferroelectric defect-free matrix [29]. The energy levels associated to the possible positions of the oxygen vacancy are three for PFZT, as may be seen in figure 4 (top left). The dipolar energy associated to the current position of the oxygen vacancy and the opposite face position in the figure are related, while the other position is fourfold and can be chosen as zero dipolar energy.

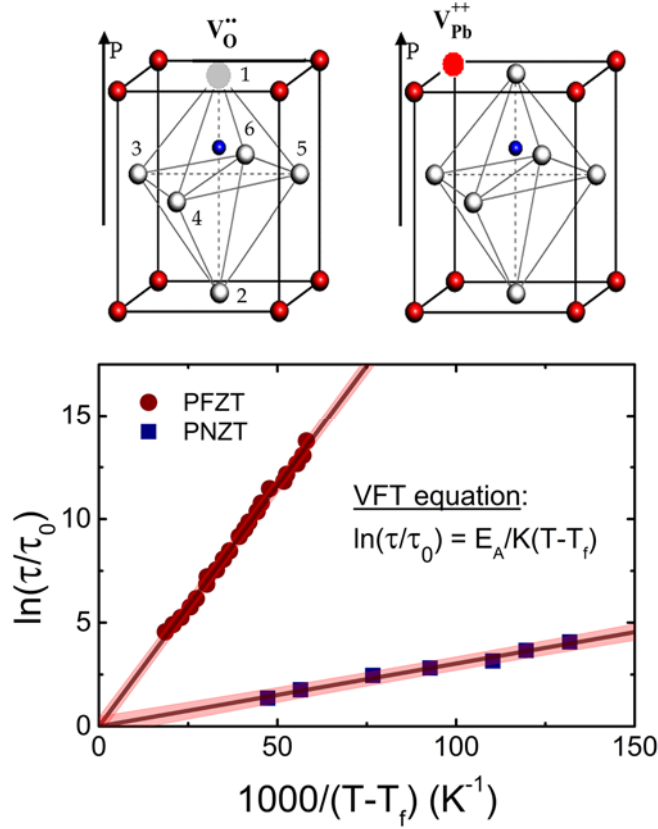


Figure 4. Dielectric relaxation data linearized according to the Vogel-Fulcher-Tammann (VFT) phenomenological equation. The values of the relaxation times, τ , are obtained from the frequencies at which permittivity was measured, while the temperatures, T , correspond to the values at which the maximum of imaginary permittivity occurs. The solid lines are a graphical representation of the linear data fit. The confidence bands at 95% (confidence level) are also shown. On the upper part of the graph, a schematic representation of the defects in the tetragonal perovskite $\text{Pb}(\text{Zr},\text{Ti})\text{O}_3$ (ABO_3) unit cell is shown, where the lattice polarization is represented by an arrow. The oxygen vacancy (on the left), formed by acceptor doping, may occupy three non-equivalent positions in the lattice; i.e., positions 1 and 2, which are different related to the B-site, and positions 3-6, which are equivalent to each other. The lead vacancy (on the right), formed by donor doping, may occupy any A-site position of the lattice. The B-sites (blue dots near the lattice center) of the $\text{Pb}(\text{Zr},\text{Ti})\text{O}_3$ lattice are regularly occupied by Zr^{4+} or Ti^{4+} , but eventually by Fe^{3+} or Nb^{5+} , depending on doping.

The dipolar moment of the $\text{Fe}'_{\text{B-site}} - \text{V}_\text{O}^{\prime\prime}$ defect can be calculated as:

$$p_i = \sum_i q_i(r_i - r) = 2e \frac{c}{4} - e \left(-\frac{c}{4} \right) = \frac{3}{4} ec$$

where c is the lattice parameter and e the electron charge, resulting in $p_i = -4.8 \cdot 10^{-29}$ C m.

The internal electric field can be estimated from [29]:

$$E_i = \frac{P_s}{2\epsilon_0\epsilon_M}$$

where $\varepsilon_M = 250$ is the intrinsic dielectric constant, which is obtained from the extrapolation of the ε' versus temperature curve for $T = 0$ K. This value is frequency-independent and does not depend on doping. P_S is the spontaneous polarization of the ferroelectric matrix (i.e., a dipolar defect-free material). PNZT, which has a $P_S = 30 \mu\text{C}/\text{cm}^2$ in the anomaly temperature range [30], is taken here as a ferroelectric matrix because of its dipolar defect-free nature. This value of P_S leads to an internal field $E_i = 6.8 \cdot 10^7 \text{ V m}^{-1}$. Finally, the energy level for switching the lattice polarization is:

$$W_{PFZT} = -\vec{p}_i \vec{E}_i = 20 \text{ meV}$$

The result matches the experimentally obtained activation energy for PFZT, leading to the conclusion that the thermally activated process involved may be related to polarization fluctuations due to jumps in the oxygen vacancy between the fourfold position and one of the other two of the unit cell.

In the case of PNZT, Chandrasekaran et al. [31] concluded that the associated defect between the niobium substitutional ion and lead vacancy ($Nb_{B-site}^{\cdot} - V_{Pb}''$) shows no binding energy and no preferential alignment with the polarization. Hence, this defect is unlikely to exist, and even if such complex defects do exist, it is clear that they do not interact strongly with the lattice polarization. The frequency dispersion emerges in PNZT at temperatures higher than room temperature. At these temperatures, the thermally activated motion of domain walls may cause local fluctuation of the polarization when the domain wall repeatedly exceeds the defects. This effect may be responsible for the observed dielectric dispersion in this material.

In summary, synchrotron X-ray diffraction measurements are performed in order to gain insight into the origin of the dielectric relaxation appearing in ordinary ferroelectrics at low temperatures. Results indicate that such a phenomenon is not related to crystallographic or domain configuration changes. Hence, we hypothesize that the observed phenomenon is due

to changes in the dynamic behavior of the ferroelectric domains associated with the fluctuation of the local polarization. The Vogel-Fulcher-Tammann equation is then used to estimate the activation energy of the dynamic process involved by fitting the relaxation data. The values thereby obtained depend on the nature of the existing defects in the ferroelectric matrix. On the one hand, when dipolar defects are dominant, the thermally activated oxygen vacancy jump seems to be the mechanism responsible for the polarization fluctuation. On the other hand, when only point defects are present, the thermally activated motion of domain walls could cause local fluctuation of the polarization. Other experiments may contribute to go further about the rightful origin of the observed dielectric relaxation. For instance, studying the effect of the stress and the electric field on the dielectric relaxation characteristics as well as characterizing the local structure by means of the pair distribution function (PDF) technique.

Acknowledgement

This work was supported by the MINECO (Spanish Government) project MAT2013-48009-C4-P-2. This research used resources of the Advanced Photon Source, a U.S. Department of Energy (DOE) Office of Science User Facility operated for the DOE Office of Science by Argonne National Laboratory under Contract No. DE-AC02-06CH11357. G.E. and J.L.J. acknowledge support from the U.S. National Science Foundation under award number DMR-1409399.

References

- [1] Damjanovic D 1998 *Rep. Prog. Phys.* **61** 1267
- [2] Garcia J E, Perez R, Ochoa D A, Albareda A, Lente M H and Eiras J A 2008 *J. Appl. Phys.* **103** 054108
- [3] Bokov A A and Ye Z-G 2012 *J. Adv. Dielectr.* **2** 1241010
- [4] Garcia J E, Gomis V, Perez R, Albareda A and Eiras J A 2007 *Appl. Phys. Lett.* **91** 042902
- [5] Perez-Delfin E, Garcia J E, Ochoa D A, Perez R, Guerrero F and Eiras J A 2011 *J. Appl. Phys.* **110** 034106
- [6] Zhang Q M, Wang H, Kim N and Cross L E 1994 *J. Appl. Phys.* **75** 454
- [7] Sheen D and Kim J-J 2003 *Phys. Rev B* **67** 144102
- [8] Rossetti G A, Zhang W and Khachatryan A G 2006 *Appl. Phys. Lett.* **88** 072912
- [9] Noheda B, Cox D E, Shirane G, Guo R, Jones B and Cross L E 2000 *Phys. Rev. B* **63** 014103
- [10] Lanfredi S, Lente M H and Eiras J A 2002 *Appl. Phys. Lett.* **80** 2731
- [11] Ochoa D A, Garcia J E, Perez R, Gomis V, Albareda A, Rubio-Marcos F and Fernandez J F 2009 *J. Phys. D: Appl. Phys.* **42** 025402
- [12] Lente M H, Zanin A L, Andreetta E R M, Santos I A, Garcia D and Eiras J A 2004 *Appl. Phys. Lett.* **85** 982
- [13] Lima-Silva J J, Guedes I, Filho J M, Ayala A P, Lente M H, Eiras J A and Garcia D 2004 *Solid State Commun.* **131** 111
- [14] La-Orauttapong D, Noheda B, Ye Z-G, Gehring P M, Toulouse J, Cox D E and Shirane G 2002 *Phys. Rev. B* **65** 144101
- [15] Guo H Y, Lei C and Ye Z-G 2008 *Appl. Phys. Lett.* **92** 172901
- [16] Alguero M, Jimenez R, Amorin H, Vila E and Castro A 2011 *Appl. Phys. Lett.* **98** 202904
- [17] Noheda B, Wu L and Zhu Y 2002 *Phys. Rev. B* **66** 060103R
- [18] Jaffe B, Cook W R and Jaffe H 1971 *Piezoelectric Ceramics* London Academic Press
- [19] Eichel R A 2007 *J. Electroceram.* **19** 9
- [20] Daniels J E, Jones J L and Finlayson T R 2006 *J. Phys. D: Appl. Phys.* **39** 5294

- [21] Ochoa D A, Esteves G, Iamsasri T, Rubio-Marcos F, Fernández J F, Garcia J E and Jones J L 2016 *J. Eur. Ceram. Soc.* **36** 2489
- [22] Arlt G, Hennings D and de With G 1985 *J. Appl. Phys.* **58** 1619
- [23] Ren S, Lu C, Liu J, Shen H and Wang Y 1996 *Phys. Rev. B* **54** R14337
- [24] Niermann D, Waschkowski F, de Groot J, Angst M and Hemberger J 2012 *Phys. Rev. Lett.* **109** 016405
- [25] Sippel P, Krohns S, Thoms E, Ruff E, Riegg S, Kirchhain H, Schrettle F, Reller A, Lunkenheimer P and Loidl A 2012 *Eur. Phys. J. B* **85** 235
- [26] Zhou Y, Chan H K, Lam C H and Shin F G 2005 *J. Appl. Phys.* **98** 034105
- [27] Zhou Y and Shin F G 2006 *J. Appl. Phys.* **100** 024101
- [28] Zhou Y 2010 *Solid State Commun.* **150** 1382
- [29] Arlt G and Neumann H 1988 *Ferroelectrics* **87** 109
- [30] Garcia J E, Ochoa D A, Gomis V, Eiras J A and Perez R 2012 *J. Appl. Phys.* **112** 014113
- [31] Chandrasekaran A, Damjanovic D, Setter N and Marzari N 2013 *Phys. Rev. B* **88** 214116